Marine Chemistry 161 (2014) 1–13

Contents lists available at ScienceDirect

Marine Chemistry

journal homepage: www.elsevier.com/locate/marchem

Seasonal variability of aragonite saturation state in the Western Pacific

Mareva Kuchinke [a,*], Bronte Tilbrook [a,b,c], Andrew Lenton [a]

[a] Centre for Australian Weather and Climate Research, CSIRO Marine and Atmospheric Research, Hobart, Tasmania, Australia
[b] CSIRO Wealth from Oceans National Research Flagship, PO Box 1538, Hobart, TAS 7001, Australia
[c] Antarctic Climate and Ecosystems CRC, Hobart, TAS 7001, Australia

ARTICLE INFO

Article history:
Received 24 May 2013
Received in revised form 19 December 2013
Accepted 7 January 2014
Available online 24 January 2014

Keywords:
Aragonite saturation state
Seasonal variability
Surface tropical Pacific Ocean
Processes
Precipitation
Advection
Upwelling

ABSTRACT

The oceanic uptake of atmospheric carbon dioxide (CO_2) since pre-industrial times has increased acidity levels, resulting in a decrease in the pH and aragonite saturation state (Ω_{ar}) of surface waters. Aragonite is the predominant biogenic form of calcium carbonate precipitated by calcifying organisms in tropical reef ecosystems. Values of Ω_{ar} are often used as a proxy for estimating calcification rates in corals and other calcifying species. We quantify the regional and seasonal variability of Ω_{ar} and its main drivers for the Pacific island region (120°E:140°W, 35°S:30°N). The calculation of Ω_{ar} uses a seasonal climatology of the surface-water partial pressure of CO_2, combined with values of total alkalinity (TA) estimated from a relationship between surface water salinity and total alkalinity that is derived from measurements in the region. This relationship is valid for all phases of El Niño/Southern Oscillation and for mixed layer waters with less than 15 μmol kg^{-1} dissolved nitrate.

The influence of seasonal changes in sea surface temperature (SST) on Ω_{ar} is small except in the subtropical waters on the northern and southern boundaries of the study region. Here, SST seasonal variability is large (>5 °C), causing a change in Ω_{ar} of greater than 0.1. Seasonal changes in mixed layer depth and net evaporation (precipitation) do influence the seasonality in TCO_2 and TA. However, these processes tend to increase (decrease) the TCO_2 (TA) in unison, resulting in a small net effect on seasonal change in Ω_{ar} for most of the region. Net biological production and sea–air gas exchange were also found to have only a small impact on the seasonal change in Ω_{ar} through the region. Changes in Ω_{ar} of between 0.1 and 0.2 occurred where variations in wind-driven upwelling in the Central Equatorial Pacific and the transport of Eastern Pacific waters into the South Equatorial Current region caused a change in the TCO_2/TA ratio of the surface waters. In contrast to these two regions, the combined effect of biological and physical processes in the West Pacific Warm Pool and North Equatorial Counter Current subregions resulted in Ω_{ar} variability of less than 0.1.

1. Introduction

Since the start of the industrial revolution, about 48% of the anthropogenic CO_2 emitted to the atmosphere has been taken up and stored in the ocean (Sabine et al., 2004). The CO_2 taken up by the ocean reacts in seawater, causing decreases in pH and dissolved carbonate ion concentrations (CO_3^{2-}), with the changes collectively referred to as ocean acidification (e.g. Caldeira and Wickett, 2003).

Ocean acidification is expected to reduce calcification in reef ecosystems (Hoegh-Guldberg et al., 2007; Langdon et al., 2000; Orr et al., 2005), may alter nutrient speciation and availability (Dore et al., 2009), and potentially change phytoplankton species composition and growth (Fabry et al., 2008; Iglesias-Rodriguez et al., 2008). Many marine calcifying organisms such as corals, calcareous algae, and mollusks, tend to exhibit a reduced capacity to build their shells and skeletons under more acidic conditions (Doney et al., 2012). Ocean acidification, in conjunction with additional stresses such as ocean warming, has implications for the health and longer-term sustainability of reef ecosystems (Silverman et al., 2009) with potential to impact fisheries, aquaculture, tourism, and coastal protection (e.g. Cooley et al., 2009).

In the tropical Pacific Ocean, the increase of atmospheric CO_2 concentrations for the period 1750–1995 is estimated to have resulted in a decrease in surface water CO_3^{2-} from ~270 μmol kg^{-1} to ~225 μmol kg^{-1} (Feely et al., 2009). For a high CO_2 emission scenario such as A2 (Nakicenovic et al., 2000), the atmospheric CO_2 concentration is predicted to be about 850 ppm by 2100, which is projected to lead to a decrease in CO_3^{2-} to ~140 μmol kg^{-1} (Feely et al., 2009).

The decrease in the dissolved carbonate ion concentration that occurs through ocean acidification results in a decrease in the aragonite saturation state (Ω_{ar}) of the waters:

$$\Omega_{ar} = \frac{\left[Ca^{2+}\right]\left[Co_3^{2-}\right]}{K_{sp}^{*}} \quad (1)$$

* Corresponding author.
E-mail address: mkuchinke@gmail.com (M. Kuchinke).

http://dx.doi.org/10.1016/j.marchem.2014.01.001

where $[Ca^{2+}]$ and $[CO_3^{2-}]$ are the concentrations of dissolved calcium and carbonate ions respectively, and K^*_{sp} is the solubility product at in situ sea surface temperature (SST) and salinity (SAL) and one atmosphere pressure (Mucci, 1983).

Aragonite is a metastable form of calcium carbonate that is produced by major calcifiers in coral reef ecosystems, including the reef building corals, and is the predominant biogenic carbonate mineral in warm and shallow waters of the tropics (Stanley and Hardie, 1998). The aragonite saturation state of seawater has been used as a proxy for the estimation of net calcification rate for corals (e.g. Gattuso et al., 1998; Langdon et al., 2000). Langdon and Atkinson (2005) estimated a decrease of 1 unit of Ω_{ar} relates to about 28% decline in net coral calcification rate, although a uniform response is not observed for all coral species.

The Ω_{ar} of tropical Pacific surface water is estimated to have decreased from values of about 4.5 in pre-industrial times (Cao and Caldeira, 2008; Guinotte et al., 2003; Kleypas et al., 1999) to about 3.8 by 1995 (e.g. Feely et al., 2009). Regional and seasonal variabilities of CO_2 system parameters that can influence Ω_{ar} values have been documented for the study area, although not in terms of understanding the regional variability of Ω_{ar}. These CO_2 system parameters are the partial pressure of CO_2 (pCO_2, Feely et al., 2002; Inoue et al., 2003, 1995; Ishii et al., 2009; Takahashi et al., 2009), total dissolved inorganic carbon dioxide (TCO_2, Ishii et al., 2001), total alkalinity (TA, Lee et al., 2006), sea surface temperature (SST, Johnson et al., 2002), and sea surface salinity (SAL, Bingham et al., 2010; Johnson et al., 2002).

Here, we use a surface pCO_2 climatology and derive an updated relationship between measured TA and SAL to provide two CO_2 system parameters that can be used to calculate other carbonate chemistry parameters including, aragonite saturation state and TCO_2. These data are used to quantify for the first time the magnitude of regional and seasonal variability in aragonite saturation state and the processes driving this variability in the Pacific Island region.

2. Methods

2.1. The setting

Our study covers surface seawater (pressure ≤10 dbar) in the region delimited by 120°E:140°W and 35°S:30°N. This region includes many Pacific Island nations and contains a number of surface water masses influenced by major currents (Fig. 1). The following discussion on the temporal and spatial variability of the CO_2 system parameters firstly considers the whole Pacific study area. More detailed discussion of the factors controlling the variability in Ω_{ar} for the four subregions that characterize major water masses of the study area is presented. These subregions are described below and are the Western Pacific Warm Pool, the Central Equatorial Pacific, and two areas north and south of the Equator.

Western Pacific Warm Pool (WPWP, 0°:8°N, 142.5°E:162.5°E): The WPWP subregion is characterized by sea surface temperature (SST) values greater than 29 °C and surface salinities less than 34 (McPhaden and Picaut, 1990; McPhaden, 1999). The entire WPWP is usually found between about 120°E to 160°E and 8°S to10°N. On interannual time scales and under El Niño conditions, the WPWP can extend eastward as far as 140 °C (McPhaden and Picaut, 1990; McPhaden, 1999). During the summer monsoon season, greater precipitation lowers the salinity and the density of the surface seawater leading to a thickening of a barrier layer (De Boyer Montégut et al., 2007) that limits the exchange of CO_2 and nutrients between the mixed layer and deeper water (Feely et al., 2002; Ishii et al., 2001; Le Borgne et al., 2002). The partial pressure of CO_2 in surface waters is similar to atmospheric values and the net exchange of CO_2 across the sea–air interface is small (Ishii et al., 2001; Ishii et al., 2009).

Central Equatorial Pacific (CEP, 4°S:4°N, 157.5°W:142.5°W): The CEP is east of the WPWP. The southeast trade winds are strongest

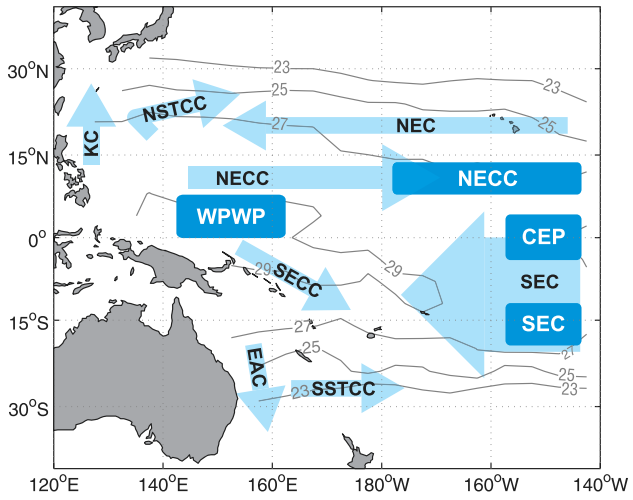

Fig. 1. Main surface currents in the Pacific island region with contours of the annual mean climatology of SST (modified after Ganachaud et al. (2012)). Surface currents are represented by the light blue arrows while the sub-regions are the blue boxes. NSTCC = North Sub-Tropical Counter Current, NEC = North Equatorial Current, NECC = North Equatorial Counter Current, SEC = South Equatorial Current, SECC = South Equatorial Counter Current, SSTCC = South Sub-Tropical Counter Current, KC = Kuroshio Current, EAC = East Australian Current. The West Pacific Warm Pool (WPWP) is located where SST > 29 °C.

from June to September, followed by a strengthening of the northeast trade winds from November to February. The increased strength of the trade winds causes enhanced upwelling of waters from the upper thermocline in this region (Reverdin et al., 1994; Wang et al., 2000). This upwelling brings cooler and saltier waters, higher in TCO_2, TA, and pCO_2 (Wanninkhof et al., 1995) to the surface and the sea to air flux of CO_2 to the atmosphere is highest during these periods (Takahashi et al., 2009). This upwelling is stronger under La Niña compared to El Niño conditions (Philander, 1990).

North Equatorial Counter Current (NECC, 8°N:12°N, 177.5°W:142.5°W): The NECC is to the north of the CEP and has an annual mean position centered at about 10°N. The NECC is an eastward extension of the relatively low salinity WPWP waters, and typically has a salinity of about 34.5 with a seasonal variability of about 0.4. From July to November, the salinity within the region decreases due to the summer monsoon bringing warmer and fresher waters from the west and as the core of the NECC shifts closer to the equator. The TCO_2, TA, and pCO_2 values decrease to the west towards the WPWP (Ishii et al., 2009) and the greater eastward transport of the NECC from July to November is likely to lower TCO_2 and TA in the sub-region.

South Equatorial Current (SEC: 20°S–12°S, 157.5°W–142.5°W): The SEC flows west as part of the South Subtropical Gyre and can extend from 5°N to 20°S (Ganachaud et al., 2012). The SEC usually is found down to 100 to 200 m depth (Reverdin et al., 1994). The seasonal variability of the southeast and northeast trade winds affects SST, SAL (Bingham et al., 2010), pCO_2 (Feely et al., 2002; Takahashi et al., 2009), TA, and TCO_2 (Wanninkhof et al., 1995) of surface waters. In the SEC sub-region, the strengthening of the trade winds enhances evaporative cooling and upwelling, leading to cooler and higher salinity waters (Bingham et al., 2010), which may cause TA to increase following Eq. (2), and the calculated TCO_2 from TA and pCO_2 to also increase.

2.2. Calculated TCO_2 and Ω_{ar}

The TCO_2 and Ω_{ar} values are calculated using pCO_2 and TA, along with the seawater temperature and salinity and the thermodynamic constants for carbonic acid (Park, 1969). We used the Takahashi et al. (2009)

climatology for surface SST, SAL and pCO_2. This monthly 4° × 5° climatology for pCO_2 is based on surface underway measurements corrected to the year 2000, with data collected in the 10°S to 10°N band during El Niño events excluded from the data set (Fig. 2a).

The coverage of TA is less extensive (Fig. 2b). Equations to calculate TA from SAL and SST in the Pacific Ocean have been derived by Chen and Pytkowicz (1979), Millero et al. (1998), Lee et al. (2006), and Christian et al. (2008). The Chen and Pytkowicz data were from the 1970's Pacific Geochemical Ocean Sections Study and Lee et al. used data collected prior to 2006. We re-evaluated the relationship of TA to salinity and SST using a larger and more recent dataset collected on high-resolution hydrographic sections (Fig. 2, Table 1). These data were sourced from the CLIVAR and Carbon and Hydrographic Data Office (http://cchdo.ucsd.edu/), and cover a greater range of years and multiple La Niña and El Niño events. This allowed us to assess how these events might influence the relationship between TA and SAL, and if the relationship was compatible with the Takahashi climatology that excluded equatorial data collected in El Niño years.

The pCO_2, SAL, and SST values from the LDEOv2009 climatology (Takahashi et al., 2010), and calculated TA values described below were used with CO2SYS (Van Heuven et al., 2009) to estimate TCO_2 and Ω_{ar}. The carbonic acid dissociation constants of Millero et al. (2006) were used for the calculation as the estimated errors for these thermodynamic constants are considered to be smaller compared to other published constants (Millero et al., 2006). For the calculation of Ω_{ar} (Eq. (1)), the concentration of dissolved calcium ions in μmol kg^{-1} is estimated from salinity using $[Ca^{2+}] = 2.934 \times 10^{-4}SAL$ (Culkin and Cox, 1976). The concentration of carbonate ion $[CO_3^{2-}]$ is a function of TA and TCO_2 at a given SST and SAL, and K^*_{sp} is a function of SST and SAL.

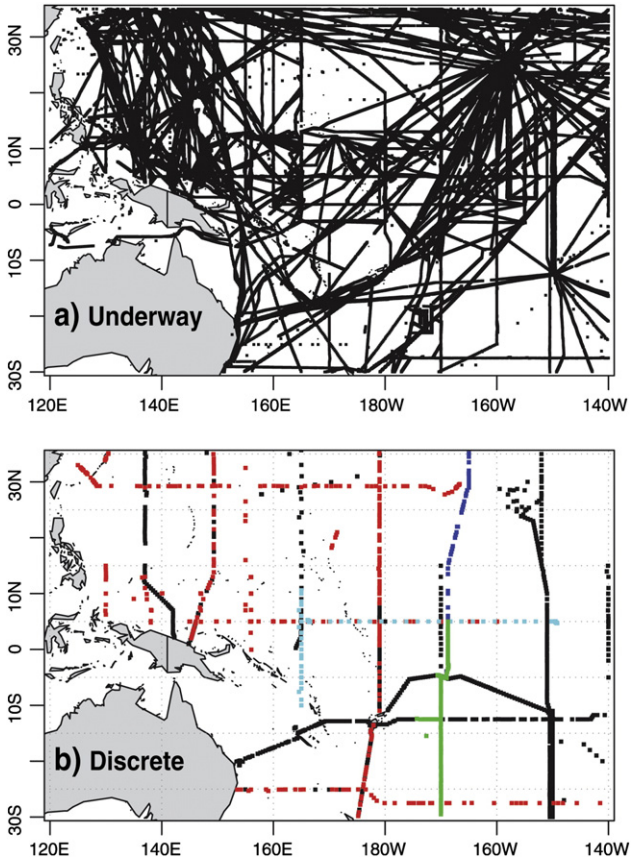

Fig. 2. a) Ship tracks between 1968 and 2008 where continuous pCO_2, SST and SAL were collected simultaneously. Data are those from the LDEO database V2009 (Takahashi et al., 2010) obtained from the Carbon Dioxide Information Analysis Center (CDIAC). b) Stations occupied between 1990 and 2009 by the U.S. (black), Japan (red), Australia (green), Canada (dark blue), and France (cyan). Voyages are listed in Table 1.

Table 1
Number of discrete TCO_2 and TA measurements in the top 10 dbar given in μmol kg^{-1}. Numbers in the neutral, La Niña, and El Niño columns are the number of either TCO_2 or TA samples collected during the corresponding oceanic condition based on the Oceanic Niño Index of the Nino 3.4 and Nino 4 regions. The number of samples collected outside these 2 regions is in the column "Outside".

Voyage code	Country	TCO_2	TA	Outside	Neutral	La Niña	El Niño
EQF_1992	USA		9	2	7		
EQS_1992	USA		55	17			38
FLUPAC_1994	France	70	67	9			62
MP_5_2002	USA	10	10	10			
MP_6_2002	USA	1	1	1			
MR00_K08	Japan	8		4		4	
MR02_K02	Japan	9		2	7		
MR02_K06_LEG34	Japan	2					2
MR03_K02	Japan	6	6	6			
MR04_07	Japan	10	10	10			
MR98_K02	Japan	4				4	
MR99_K06	Japan	13		13			
MR99_K07	Japan	8		4		4	
P02T_1994	USA	1	1	1			
P03_2005_LEG2[a]	Japan	26	25	26			
P03_2005_LEG3[a]	Japan	8	8	8			
P06E_2003	Japan	1	1	1			
P06W_1992	USA	5		5			
P06W_2003[b]	Japan	11	11	11			
P08S_1996[c]	Japan	2	1	2			
P09_1994[d]	Japan	32	9	32			
P10_1993	USA	16	17	17			
P10_2005[e]	Japan	22	22	22			
P13N_1992	USA	37	37	22	16		
P14_LEG1_2007[f]	Japan	14	14	14			
P14_LEG2_2007[f]	Japan	27	27	21		6	
P14N_1993	USA	23	22	8	15		
P14S_P15S_1996	USA	64	61	61		4	
P15S_2001	Australia	85	83	75	10		
P15S_2009	Australia	81	88	77		11	
P16A_P17A_1992	USA	6	6	6			
P16C_1991	USA	19	20	12			8
P16N_1991	USA	9		9			
P16N_2006	USA	54	51	40		15	
P16S_2005	USA	37	39	39			
P16S_P17S_1991	USA	35	38	38			
P21_1994	USA	33	38	38			
P31_1994	USA	23	23	26			
PR06_P15N_1994	Canada	28	25	21			7
Total		840	825	710	55	48	117
Total samples = 930[g]				76%	6%	5%	13%

[a] Also known as the JAMSTEC MR05_05_LEG2 and MR05_05_LEG3.
[b] Also known as the BEAGLE MR03_K04_LEG1 and MR03_K04_LEG2.
[c] Also known as the JAMSTEC K96_05.
[d] Also known as the JAMSTEC RY9407.
[e] Also known as the JAMSTEC MR05_02.
[f] Also known as the JAMSTEC MR07_06_LEG1 and MR07_06_LEG2.
[g] 930 is the total number of samples collected during neutral (55), La Niña (48), and El Niño (117) conditions, and outside (710) the Niño 4 and Niño 3.4 regions.

3. Results and discussion

This section describes the updated TA–SAL relationship, and then focuses on the estimation, variability and distribution of TA, TCO_2, and Ω_{ar} for the Pacific study area. The seasonal variability of pCO_2, SST and SAL has been documented for the region in previous studies (Bingham et al., 2010; Johnson et al., 2002; Takahashi et al., 2009).

3.1. TA–SAL relationship

For the Pacific Ocean study region, the GLODAP and CLIVAR TA and SAL data (http://cchdo.ucsd.edu/pacific.html) were used to derive the following relationship:

$$TA_{calc} = (2300.0 \pm 0.2) + (66.3 \pm 0.4) \times (SAL - 35). \quad (2)$$

The standard error of the fit is ±6 μmol kg^{-1} and the coefficient of determination $R^2 = 0.98$. An SST term in (2) reduced the residuals by only 0.1%, and was not included in the equation. The TA–SAL relationship is compared to earlier relationships (Chen and Pytkowicz, 1979; Christian et al., 2008; Lee et al., 2006) in Fig. 3. The TA residuals in Fig. 3 are the difference between the measured TA values for surface samples from the GLODAP and CLIVAR/CO_2 section data and the derived TA values. The variance of the residuals is indicated by the slope of the lines. The range of the residuals should be small and the variance constant (i.e. little or no gradient) if the relationship is a good predictor of TA. Comparison of the measured and calculated TA from (2) shows the residuals range from −20 to 20 μmol kg^{-1}.

Most of the surface samples used to calculate the TA–SAL relationship are from nutrient-poor, oligotrophic waters in the Pacific study area. The effect of dissolved nitrate on TA (Brewer and Goldman, 1976) was estimated using surface (<10 dbar) data from the CLIVAR/CO_2 Pacific Ocean sections P06 and P21. These cruise data were collected after 2008 and were not used to calculate the relationship in Eq. (2). The TA residuals average −5.8 ± 3.9 μmol kg^{-1} (n = 117) for leg 1 of P06 along 30°S, and −3.2 ± 6.0 μmol kg^{-1} (n = 8) for leg 2 of P21 between 17°S and 25°S. The surface nitrate concentrations for the TA samples used were less than 5 μmol kg^{-1}. In subsurface waters, when nitrate concentrations exceed about 15 μmol kg^{-1}, the TA residuals from (2) when compared to measurements are greater than twice the standard error of TA_{calc} fit (2σ = 12 μmol kg^{-1}). The greater residuals in the deeper waters could result from dissolution of carbonate minerals and contributions from water masses with different TA–SAL relationships. As a result, the TA–SAL relationship in (2) should only be used for mixed layer waters of the Pacific study area where nitrate concentrations are less than 15 μmol kg^{-1}.

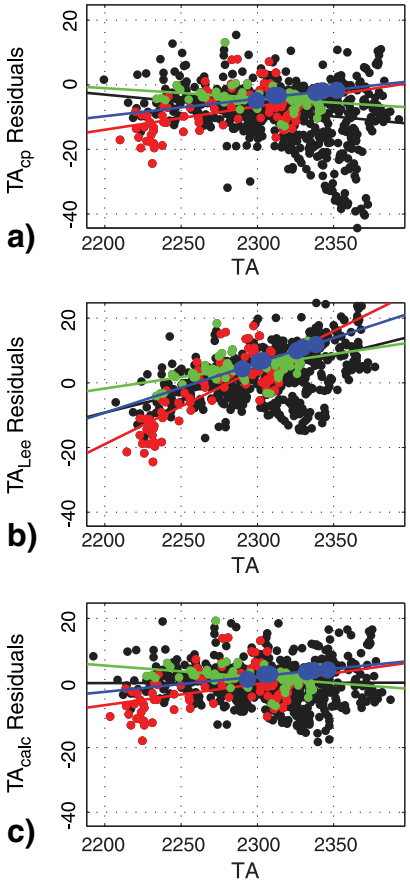

Fig. 3. The difference between observed and predicted TA (TA residuals) plotted against the predicted TA. Predicted TA values using Chen and Pytkowicz (1979) are shown on the top row (a), Lee et al. (2006) on the middle row (b), and Eq. (2) on the bottom row (c). Red dots represent samples collected during an El Niño event, blue for La Niña, green for neutral, and black for those collected outside the Niño 3.4 and Niño 4 regions.

Data used to derive the TA–SAL relationship in (2) were collected over a number of years covering El Niño and non-El Niño events (Table 1). We investigated how the time and location of sampling for TA might influence the calculated TA values by classifying measured TA surface values as collected in El Niño or non-El Niño conditions using the Oceanic Niño Index (ONI). The ONI is a three-month running mean of NOAA ERSST.v3 SST anomalies in the Niño 3.4 (5°N:5°S, 170°W:120°W) region based on the 1971–2000 period (http://www.cpc.ncep.noaa.gov/data/indices/). Data collected within the Niño 3.4 and Niño 4 (5°S:5°N, 160°E:150°W) regions were identified and assigned to El Niño events when the SST anomalies where above 0.5 °C for 3 consecutive months, or La Niña events when the SST anomalies where below 0.5 °C for 3 consecutive months. If the ONI was less than 0.5 °C over the 3 consecutive months, these values were assigned a "neutral" condition. All data collected outside of the Niño 4 and Niño 3.4 regions were considered less likely to be influence by La Niña and El Niño events and in Table 1 have been assigned as "outside". For all samples, 13% were collected during an El Niño condition, 11% during a non-El Niño condition (5% of La Niña and 6% of neutral events), and 76% were outside the Niño 3.4 and Niño 4 regions (Table 1). The TA–SAL relationship of (2) was found to be independent of the El Niño or non-El Niño conditions in the study area (Fig. 3). Thus, the Eq. (2) relationship appears to be applicable for all phases of ENSO.

The earlier relationships used to estimate TA of Chen and Pytkowicz (1979) and Lee et al. (2006) covered a greater region of the ocean and include temperature and salinity terms. The greater range of the residuals of the Chen and Pytkowicz equations (−45 to 20 μmol kg^{-1}, Fig. 3a) compared to (2) is likely due to their relationship using a limited amount of data collected between August 1973 and June 1974 during the Pacific Geochemical Ocean Section Study. The Lee et al. (2006) relationships were based on more data than Chen and Pytkowicz and the calculated TA residuals compared to measured values are smaller. However, the variance of the fit over the study region as indicated by the slopes of the lines in Fig. 3b was greater than the Eq. (2) fit (Fig. 3c). Eq. (2) is an updated version of the relationship of Christian et al. (2008), which only used data reported in the GLODAP database (http://cdiac.ornl.gov/oceans/glodap/) and (2) also includes more recent data from the CARINA database (http://cdiac.ornl.gov/oceans/). The average difference for TA values calculated by Christian et al. (2008) and the TAcalc values for Eq. (2) is 2 ± 0.2 μmol kg^{-1}.

3.2. Uncertainties in the calculated TCO_2 and aragonite saturation state

The uncertainty in the calculated TCO_2 has been assessed by comparing measured values of surface TCO_2 for the region (Table 1) with values calculated using the TA_{calc} (Eq. (2)) and the corresponding surface pCO_2 values at the time the TCO_2 measurements were made. The mean differences (measured-calculated) values of TCO_2 and Ω_{ar} are −2 ± 6 μmol kg^{-1} and −0.01, respectively, indicating the calculated values do provide a good estimate of these parameters.

3.3. Spatial and temporal variability of TA_{calc}

The annual mean and seasonal variability in TA_{calc} are shown in Fig. 4 and appear to be closely related to the variability in precipitation and in the transport of the major currents in the region. The annual mean of TA_{calc} in the SEC (5°N–20°S) and NEC (15°N–20°N) regions is above 2298 μmol kg^{-1}, which is the mean value for the entire study area. The TA_{calc} values for SEC and NEC waters decrease to the west as

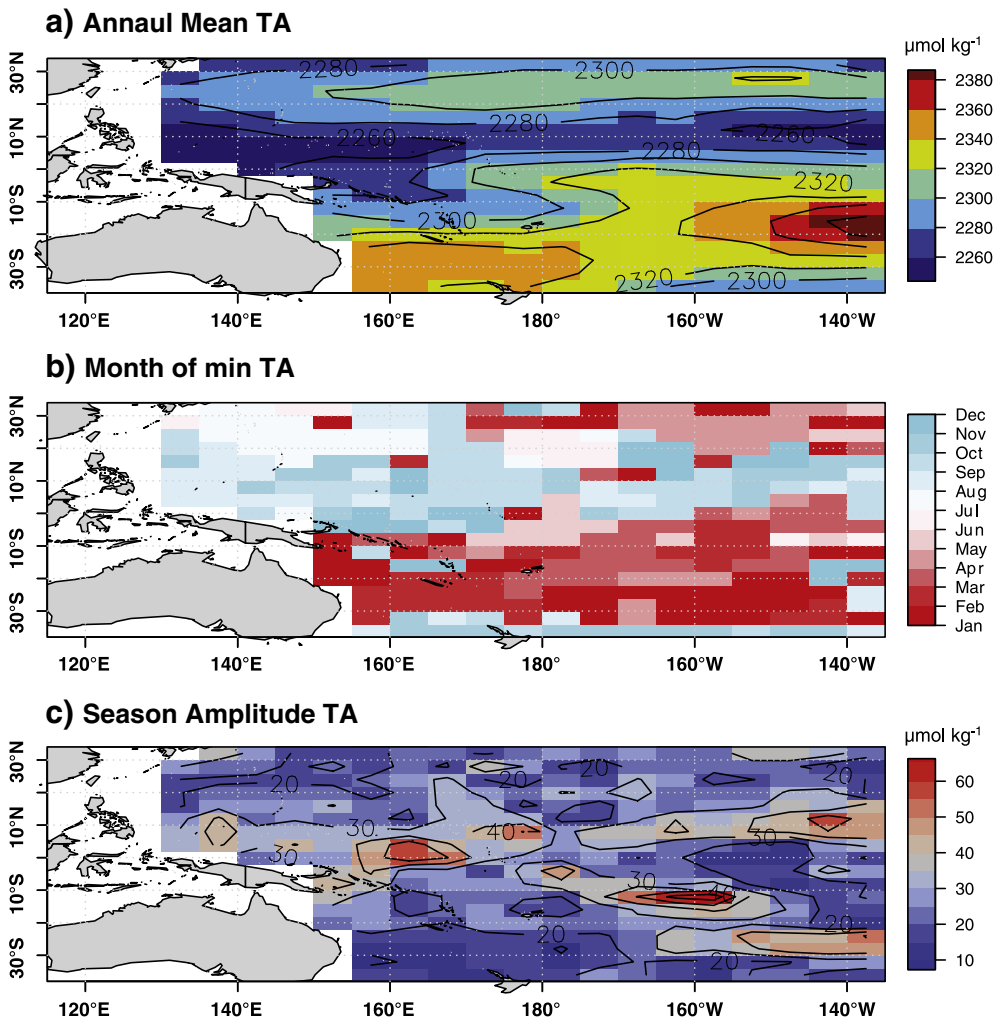

Fig. 4. For TA: a) annual mean (μmol kg^{-1}), b) month of minimum value, and c) seasonal amplitude defined as the max–min value (μmol kg^{-1}).

these waters freshen and mix more with the lower TA waters of the western Pacific.

The influence of salinity changes on surface TA values can be evaluated by normalizing the values to a constant salinity of 35 (NTA = TA × 35 / SAL) following Chen and Millero (1979). The NTA for measured samples averages 2300 ± 6 μmol kg^{-1} (n = 799) for the entire study region, in close agreement with a calculated NTA (NTA_{calc}) mean of 2300 ± 0.3 μmol kg^{-1} (n = 3708). The gridded NTA_{calc} values reported here are the same as previously reported measured NTA values (2300 ± 6 μmol kg^{-1}) of Millero et al. (1998) and is similar to the gridded NTA values (2294 ± 14 μmol kg^{-1}) calculated using interpolated surface TA from GLODAP (Key et al., 2004) and gridded salinity data from CARS (Dunn and Ridgway, 2002; Ridgway et al., 2002).

The seasonal change in salinity due to vertical mixing is typically small over the entire study area (Bingham et al., 2010), including in the equatorial and tropical Western Pacific where a semi-permanent barrier layer restricts vertical mixing (de Boyer Montégut et al., 2007). This suggests that vertical mixing has a minor role in the seasonal variability in TA, which is driven more by changes in precipitation and advection.

The months of TA_{calc} minimum values in the region of the South and North Equatorial Counter Currents (SECC and NECC, respectively) are March–April and October–December, respectively. The minima coincide with the maximum easterly transport of these currents (Chen and Qiu, 2004; Philander et al., 1987), which would result in a greater transport of fresher, low TA waters from the Western Pacific to the east. The NECC waters are also fresher and have lower TA_{calc} values than SECC waters due to greater precipitation (Bingham et al., 2010). For the WPWP, high precipitation during the summer monsoon from December to April (Bingham et al., 2010; Johnson et al., 2002) lowers salinity and results in TA_{calc} values below the annual mean (for example, TA < 2260 μmol kg^{-1} in the WPWP). The TA_{calc} minimum values in the SEC and NEC occur in March–April and in October–November, respectively, following the summer months of maximum precipitation (Bingham et al., 2010) and corresponding to the months of weakest transport (Philander et al., 1987) of higher TA waters from the east.

3.4. Spatial and temporal variability of TCO_2

The annual mean distribution of calculated TCO_2 (Fig. 5) is similar to that of TA, with a mean value of 1970 μmol kg^{-1} for the region. Values of TCO_2 above the annual mean are found in the SEC, in the South Sub-Tropical Counter Current (SSTCC), and in the north and south subtropical gyres. Values of TCO_2 below the mean are found in the NSTCC, in the SECC, and in the NECC. The TCO_2 seasonal amplitude in the SECC and NECC waters (<30 μmol kg^{-1}) is less than in the subtropical gyres, SEC, and NEC (>30 μmol kg^{-1}). Normalized values of calculated TCO_2 from Fig. 5 ($NTCO_2 = TCO_2 \times 35 / SAL$) give a mean value of 1965 ± 23 μmol kg^{-1} (n = 3708), similar to the mean for discrete measurements of 1962 ± 27 μmol kg^{-1} (n = 908). The deviations from the mean $NTCO_2$ are >23 μmol kg^{-1} compared to NTA of up to 6 μmol kg^{-1} due to air–sea exchange, biological production, and upwelling having a greater influence on TCO_2 than TA. For example, values of $NTCO_2$ along

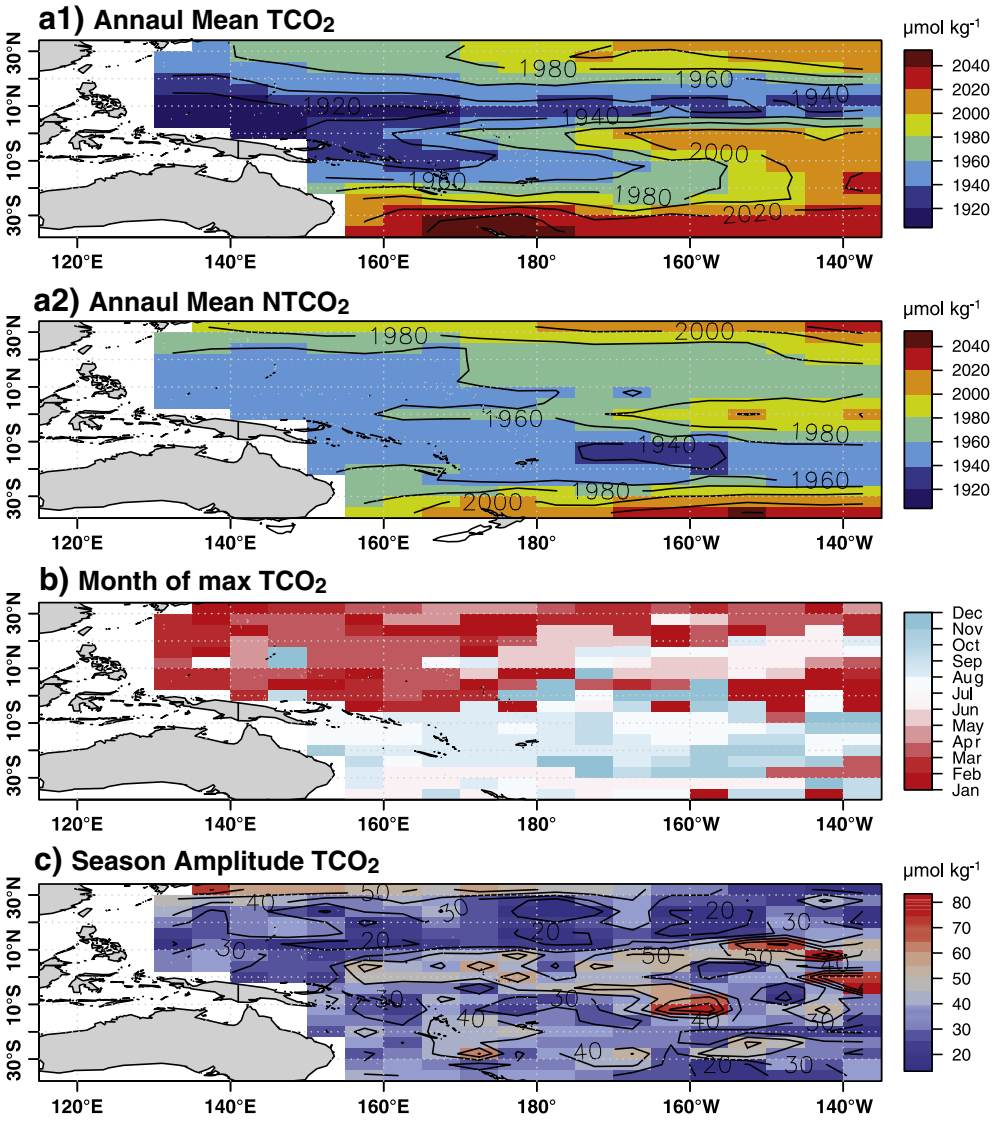

Fig. 5. For TCO_2 and $NTCO_2$ (a2): a) annual mean (μmol kg_{-1}), b) month of maximum value, and c) seasonal amplitude defined as the max–min value (μmol kg^{-1}).

the equator and east of 170°W are greater than the mean value of 1965 μmol kg^{-1} due to the upwelling of waters in the central and eastern Pacific that are relatively enriched in TCO_2. The controls on the TCO_2 distributions are discussed in more detail below.

Monthly TCO_2 changes due to sea–air exchange (SA) are estimated using the CO_2 sea–air flux climatology (F) from Takahashi et al. (2010), the mixed layer depth climatology (MLD) from De Boyer Montégut et al. (2004), and the calculated seawater density ρ from in situ SST and SAL such that $\Delta NTCO_2(SA) = F / (MLD \times \rho)$. Negative $\Delta NTCO_2(SA)$ values indicate net uptake of CO_2 by surface waters. The median monthly change in $NTCO_2(SA)$ is -0.2 μmol kg^{-1} over the entire study area. In the equatorial band and east of the dateline, the annual mean change in $NTCO_2(SA)$ is $+2 \pm 1$ μmol kg^{-1}, meaning a source of CO_2. In the counter currents and in the western tropical Pacific Warm Pool, variability in $NTCO_2(SA)$ was small. In the southern subtropical waters, the variability in $NTCO_2(SA)$ is moderate as the annual mean is -2 ± 1 μmol kg^{-1}. This means that the south subtropical waters are a sink over the entire year. The Northern Subtropical waters are a moderate source of CO_2 in the boreal summer months with a negative $NTCO_2(SA)$. The calculated $NTCO_2(SA)$ for this region is -2 ± 3 μmol kg^{-1}, in close agreement with Ishii et al. (2001). This indicates the region shifts from a sink in summer to a winter source. The results suggest that sea–air gas exchange may have a moderate effect on the annual change in $NTCO_2$ in the equatorial band to the east of the Dateline, and in the North and South subtropical waters of our study area.

The seasonal variability in MLD is no greater than about 20 m in the WPWP and a barrier layer exists at the base of the mixed layer that is considered quasi-permanent as it is present for at least 10 months per year (De Boyer Montégut et al., 2007). The depth of this barrier layer may also vary with evaporation and precipitation changes. The presence of the barrier layer in the WPWP inhibits the mixing of TCO_2 rich waters into the surface mixed layer and leads to only a small seasonal range in TCO_2 (Feely et al., 2002; Ishii et al., 2009). Outside the WPWP and the NECC regions, barrier layers are rarely detected (De Boyer Montégut et al., 2007) and deeper mixing could result in a greater seasonal change in TCO_2.

Our results show that surface NTA variations are small in time and space for the Pacific study area (NTA $= 2300 \pm 6$ μmol kg^{-1}; Fig. 4). This implies that the residence time of surface waters in the region is small enough for net $CaCO_3$ production in reefs and pelagic waters to only have a small effect on TA variability at regional scales. The TCO_2 change generated by net $CaCO_3$ production can be estimated from half the normalized alkalinity and nitrate (NNO_3) change (Chen, 1978)

such that $\Delta NTCO_2(CaCO_3) = -0.5 \times (\Delta NTA + \Delta NNO_3)$. The annual mean NO_3 concentration along the equator increases eastward from 1 to 5 μmol kg^{-1} and the rest of the region has an annual mean of 0.25 μmol kg^{-1} (Garcia et al., 2010). Hence, the annual maximum estimated $\Delta NTCO_2(CaCO_3)$ is 2.5 μmol kg^{-1}. Based on this analysis, net calcification does not appear to have a significant impact on the large seasonal or regional changes in TCO_2. However, localized calcification and production could influence TCO_2 and TA variability at the scale of coral reefs (Shaw et al., 2012).

3.5. Spatial and temporal variability of Ω_{ar} in the tropical Pacific

The averaged aragonite saturation state, Ω_{ar}, for the Pacific region is 3.8 (Fig. 6). Values of Ω_{ar} below the mean occur in the subtropical waters at the northern and southern boundaries of the study area, and in the equatorial Pacific and North Pacific to the east of 180°E (NECC and CEP). Values above 3.8 occur in the WPWP, SECC, and SEC waters between about 5°S and 25°S that are away from the influence of the equatorial upwelling in the CEP. Feely et al. (2012) calculated the aragonite saturation states using TCO_2 and TA measured on repeat hydrography sections, P06W 2003 and P16N 2006, which are within our study area. Using a 0.01/yr decrease in the aragonite saturation state (Feely et al., 2012), we can compare saturation states of these sections with the year 2000 mean values of Ω_{ar}. For example, along 160°W, surface Ω_{ar} during P16N 2006 was 3.4 ± 0.4. At a rate of −0.01/yr, Ω_{ar} would have been 3.5 ± 0.4 in 2000. This calculated value agrees with our 2000 Ω_{ar} value of 3.8 ± 0.2 within the errors of the calculations. Similarly, along 30°S, surface Ω_{ar} during P06W 2003 was 3.2 ± 0.2 and would have been about the same value in 2000, agreeing with our 2000 Ω_{ar} value of 3.7 ± 0.3.

The seasonal amplitude of Ω_{ar} is greater than 0.3 in the subtropical gyres and along the equator, whereas it is less than 0.3 in the WPWP, NECC and SECC. Minimum Ω_{ar} values for the Southern Hemisphere (except the WPWP and SECC) occur from July to December. The minima for the northern hemisphere and in the WPWP and SECC are in the January–June period (Fig. 6).

3.6. Ω_{ar} sensitivity to SAL, SST, TA and TCO_2

The effect of monthly changes in SAL, SST, TA, and TCO_2 on Ω_{ar} can be estimated from:

$$\Delta\Omega ar = \frac{\partial \Omega ar}{\partial SAL}\Delta SAL + \frac{\partial \Omega ar}{\partial SST}\Delta SST + \frac{\partial \Omega_{ar}}{\partial TA}\Delta TA + \frac{\partial \Omega ar}{\partial TCO_2}\Delta TCO_2 + \text{residuals}. \quad (3)$$

In Eq. (3), $\Delta\Omega_{ar}$ is the difference between the monthly value of Ω_{ar} and the annual mean. Each partial derivative term (e.g. $\frac{\partial \Omega ar}{\partial SAL}\Delta SAL$ or Ω_{SAL}) represents the variability of Ω_{ar} due to one parameter (e.g. SAL) while keeping the other three parameters constant in each 4° × 5° grid box. The residual term in Eq. (3) is the difference between Ω_{ar} and the sum of the partial derivative terms. The residuals range between −0.002 and 0.005 indicating that there is only a weak non-linearity in

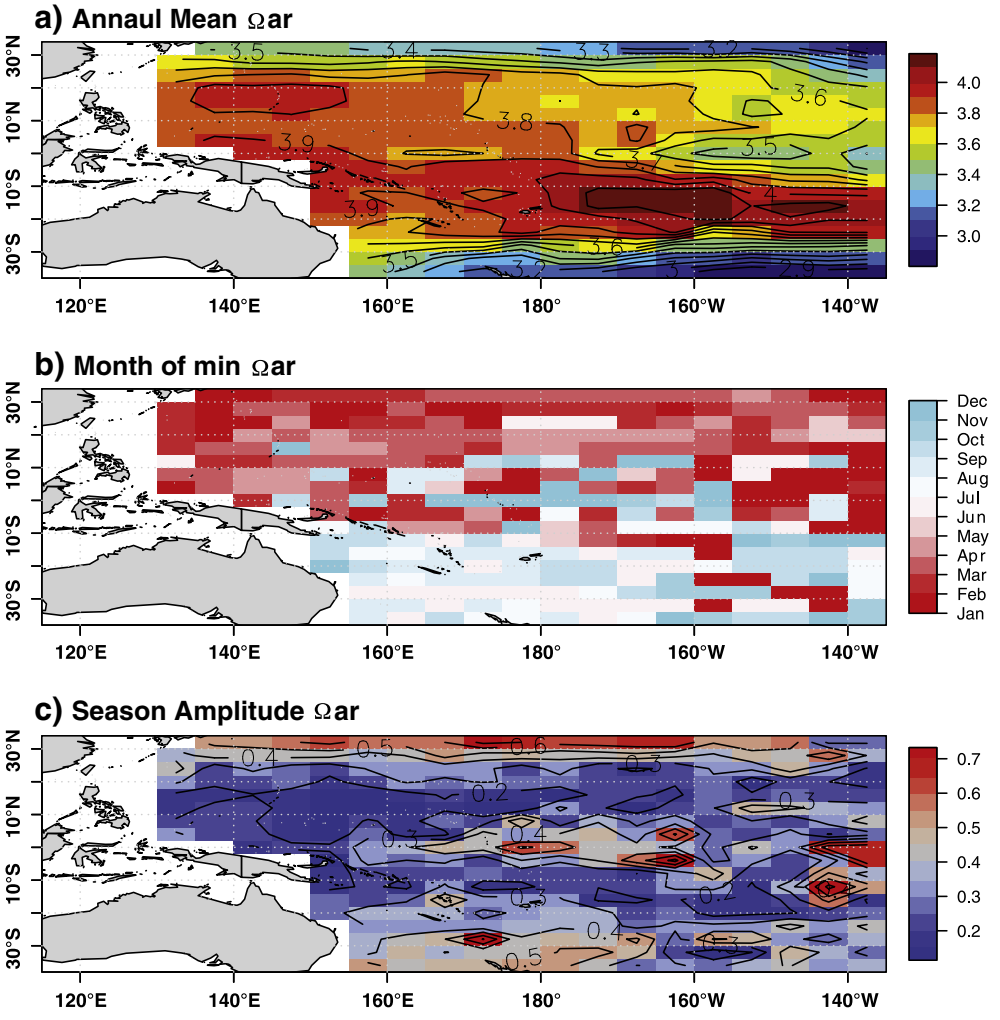

Fig. 6. For Ω_{ar}: a) annual mean, b) month of minimum value, and c) seasonal amplitude defined as the max–min value.

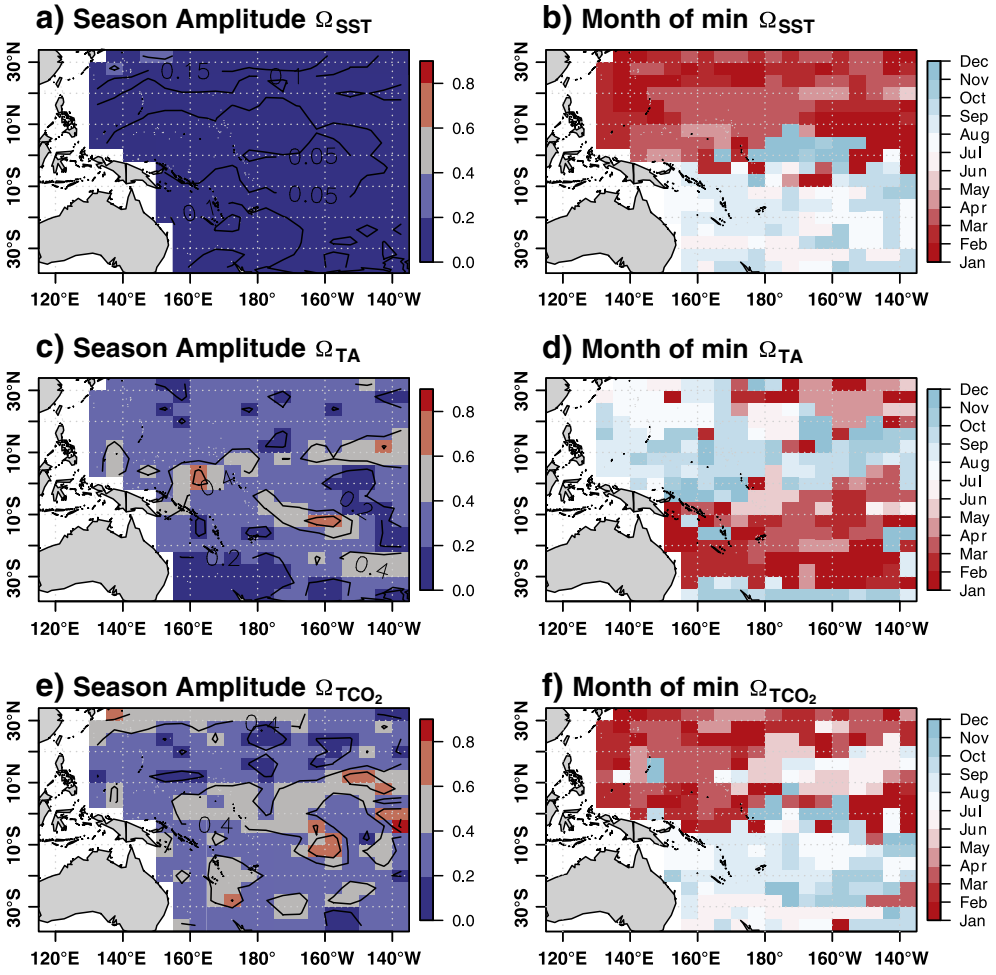

Fig. 7. Decomposition of the seasonality of Ω_{ar} with a), c), and e) the seasonal amplitude and b), d), and f) the month of minimum value. The SST, TA, and TCO_2 contribution to Ω_{ar} is given by Ω_{SST} in a) and b), by Ω_{TA} in c) and d), and by Ω_{TCO2} in e) and f), respectively. While one parameter is variable, the others are kept constants. The SAL contribution to Ω_{ar} is not shown here as the mean seasonal amplitude of Ω_{SAL} is negligible (0.02 ± 0.007).

the Ω_{ar} calculation. The results of the calculations are summarized in Fig. 7 and discussed below.

3.7. Sensitivity of Ω_{ar} to key parameters

3.7.1. Salinity

Salinity varies by −0.6 to 0.5 from the annual mean throughout the study region. This has only a small affect on $[Ca^{2+}]$ and $[CO_3^{2-}]$, and on the solubility product for aragonite, K_{sp} (Eq. (1)). The net effect of salinity in the seasonal amplitude of Ω_{ar} in Eq. (3) is small for the whole region (0.02 ± 0.007) and the direct salinity contribution to Ω_{ar} is not shown in Fig. 7. However, while the direct effect of salinity is small (0.9%), changes in salinity can have a large indirect effect on Ω_{ar} by altering the TA (Eq. (2)), as discussed below.

3.7.2. SST

The seasonal variability in SST is less than about 3 °C for most of the region between 20°N and 20°S, and SST changes of this size have only a small effect on Ω_{ar} ($\Omega_{SST} < 0.05$, Fig. 7a). Larger seasonal SST change of more than 5 °C at higher latitudes of the study area cause a greater amplitude Ω_{SST} (>0.1; Fig. 7a). Values of Ω_{SST} are minimum when SST values are lowest in the boreal winter (Jan–Mar) for the Northern Hemisphere and the austral winter (Jun–Aug) in the Southern Hemisphere (Fig. 7b).

3.7.3. TA

The seasonal amplitude of Ω_{TA} is greatest in regions with the largest seasonal amplitude of SAL, and hence TAcalc (Eq. (2)), which includes the WPWP, the SECC, and the NECC (Fig. 7c). In these regions, the surface salinity can vary seasonally by more than 0.3 due to high net precipitation in summer and from seasonal changes in the transport of currents that advect waters with different salinities into the region (Bingham et al., 2010). The lowest values in TA (and salinity) tend to occur from December to February in the SECC and from June to August in the NECC. A change of 0.3 in salinity corresponds to TA change of about 20 μmol kg^{-1} (Eq. (2)).

The timing of the Ω_{TA} minima is not uniform in the northern subtropics. The difference can be explained by the characteristics of the North Pacific Subtropical Counter Current (NSTCC) and the Hawaiian Lee Counter Current (HLCC) (Fig. 1). The NSTCC is typically located at 24°N extending from 130°E to 160°W, shifting slightly north towards the east. The HLCC extends from about 150°E to approximately 160°W and is centered at about 20°N (Kobashi and Kawamura, 2002).

The month of minima for TA and Ω_{TA} occurs in August–September as the easterly transport of the NSTCC weakens, and in January to May as the HLCC flow weakens (Kobashi and Kawamura, 2002).

In the Southern Hemisphere, values of Ω_{TA} are minimum from January to March, corresponding to times of lower TA. Over this period, seasonal precipitation tends to be greatest (Bingham et al., 2010) and the westward flow of SEC waters, which have high TA, is weakest (Johnson et al., 2002). Both processes are expected to result in lower TA values in the January to March period. The upwelling in the CEP is also weak over the same period, and less high TA water from below the mixed layers will be upwelled during these months. Further west in the SECC, the months of TA and Ω_{TA} minima correlate with the austral

summer (December–February) when high precipitation (Brown et al., 2010) will lower surface salinity and TA (Eq. (2)).

3.7.4. TCO_2

As shown in the following sections, TCO_2 is a major driver in Ω_{ar} variability throughout the region. The Ω_{TCO2} values are low in winter months when surface TCO_2 is higher due to deeper mixed layers, potentially greater net respiration in some regions (Ishii et al., 2001) or lower net primary production (Behrenfeld et al., 2005), and possibly the advection of CO_2 rich waters into a region. Values of Ω_{TCO2} vary by more than 0.3 in the equatorial zone and in the subtropical gyres where the seasonal variability of TCO_2 is greater than 20 μmol kg^{-1}. For the remainder of the study area, seasonal changes of less than 20 μmol kg^{-1} occur in TCO_2 in the WPWP, SECC and NECC and result in seasonal changes of less than 0.3 Ω_{TCO2}. These are regions of relatively low wind and high precipitation that contribute to low salinity surface and a thickening of the barrier layer, inhibiting the exchange of CO_2 between the deep and surface oceans (Ishii et al., 2001).

We now describe and discuss the relative contribution of TCO2, TA, SST and SAL changes to the seasonal Ω_{ar} variability in the Pacific sub-regions of 1) WPWP and NECC, 2) the CEP, and 3) the SEC. This sensitivity analysis uses Eq. (3) with plots for each subregion shown in Figs. 8–11. The variabilities of TCO2 and TA, and SST and SAL are paired for scaling convenience and shown in the top and middle panels respectively. These are calculated as the deviation of the monthly average values from the annual mean of each parameter. The sensitivity of Ω_{ar} to the respective parameter variability is shown in the bottom panel.

3.8. Variability in the West Pacific Warm Pool (0°:8°N 142.5°E:162.5°E) and the North Equatorial Counter Current (8°N:12°N 177.5°W:142.5°W) subregions

The variability in Ω_{ar} relative to the annual mean is low in the WPWP (±0.04, Fig. 8) and in the NECC (±0.06, Fig. 9) subregions. The TCO_2 and TA seasonal amplitudes are about 30 μmol kg^{-1} for both the WPWP (Fig. 8) and NECC (Fig. 9). Both TA and TCO_2 concentrations tend to covary and the resulting changes in Ω_{ar} over seasons are small. TCO_2 and TA minimum values occur in October with maximum values in March (WPWP; Fig. 8) and June (NECC; Fig. 9). The presence of a barrier layer inhibits the vertical mixing of both TCO_2 and TA-rich waters into the surface mixed layer and sea–air CO_2 net flux has little effect on TCO_2 (Ishii et al., 2009). The seasonal variability in salinity is largely dominated by variability in net precipitation (Bingham et al., 2010), and appears to be a key driver of the change in TCO_2 and TA in the WPWP and the NECC regions. The calculated $NTCO_2$ changes from the annual mean value by less than ±4 μmol kg^{-1} in the WPWP and ±6 μmol kg^{-1} in the NECC subregions.

3.9. Variability in the Central Equatorial Pacific (CEP) subregion (4°S:4°N 157.5°W:142.5°W)

In the CEP subregion, Ω_{ar} varies by −0.1 to +0.08 from the annual mean value between January and May, and from −0.04 to 0.04 between August and November (Fig. 10). Note that Fig. 6 shows amplitudes of Ω_{ar} as large as 0.3 in the CEP subregion, but the average across the subregion is lower. The amplitude of the TCO_2 variability from the annual mean (−10 to 12 μmol kg^{-1}) is about twice that of TA (−6 and 4 μmol kg^{-1}). For the periods December–April and in July–August the TCO_2 increases more than TA. In contrast, between May to July and September to November, TCO_2 decreases more relative to TA. The greater seasonal change in TCO_2 relative to TA explains most of the seasonal change in Ω_{ar}.

The strength of the equatorial Pacific upwelling is typically greatest in August and January, due to the strengthening of the southeast and northeast trade winds. The enhanced upwelling on the eastern Pacific increases surface salinity (Bingham et al., 2010), and the TCO_2 and TA (Wanninkhof et al., 1995) of the surface mixed layer (Fig. 10). Between the maximum mixed layer depth

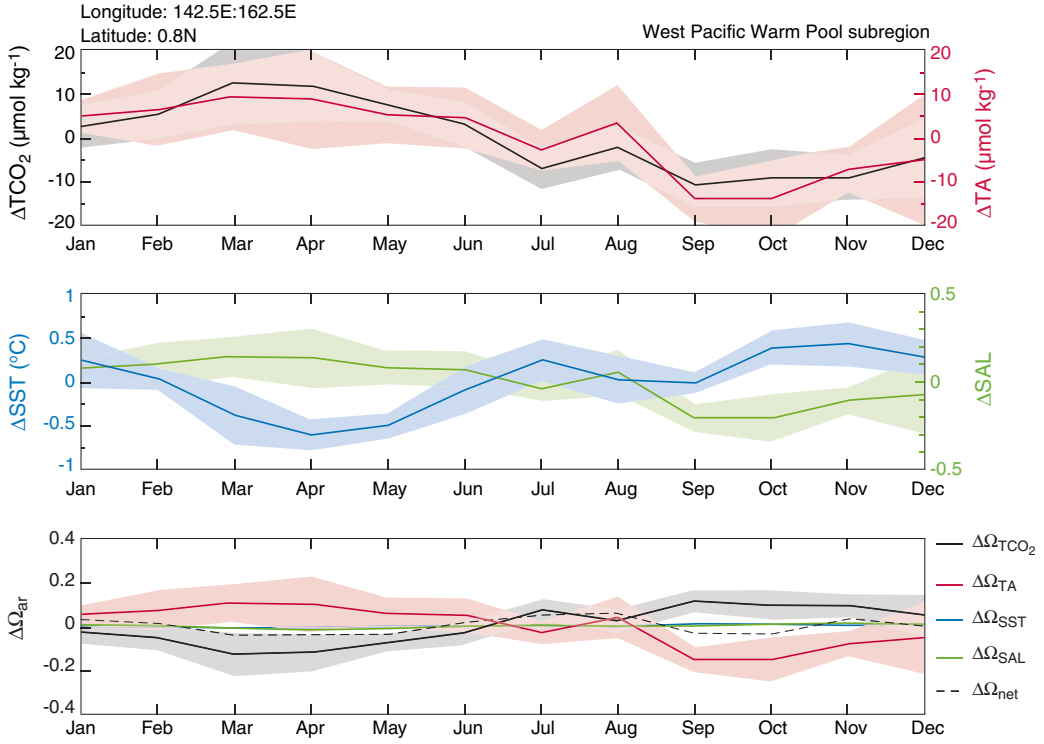

Fig. 8. In the West Pacific Warm Pool sub-region the seasonal variability with the annual mean removed in TCO_2 (black), TA (red), SST (blue), SAL (green), and their respective contribution to Ω_{ar}. The seasonality of the net effect of TCO_2, TA, SST, and SAL on Ω_{ar} is shown as a dashed line.

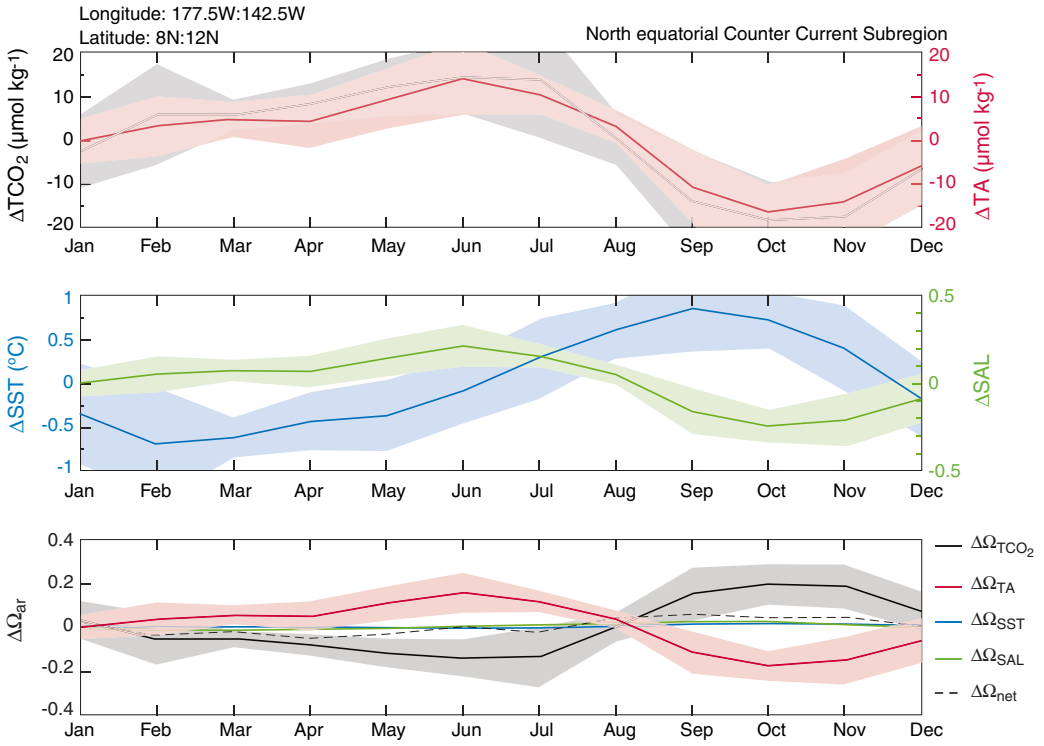

Fig. 9. In the North Equatorial Counter Current sub-region the seasonal variability with the annual mean removed in TCO_2 (black), TA (red), SST (blue), SAL (green), and their respective contribution to Ω_{ar}. The seasonality of the net effect of TCO_2, TA, SST, and SAL on Ω_{ar} is shown as a dashed line.

(~100 m) and the surface GLODAP TCO_2 varies between 30 and 68 μmol kg^{-1} depending on the location. The corresponding GLODAP TA difference is only about 9 μmol kg^{-1}. Thus periods of enhanced upwelling will increase the TCO_2 of surface waters relative to TA, leading to a lower Ω_{ar}.

3.10. Variability in the South Equatorial Current subregion (20°S:12°S 157.5°W:142.5°W)

The net annual mean Ω_{ar} fluctuates by ±0.1 in the SEC subregion and seems to be driven by the variability in TCO_2 (Fig. 11). Although TCO_2

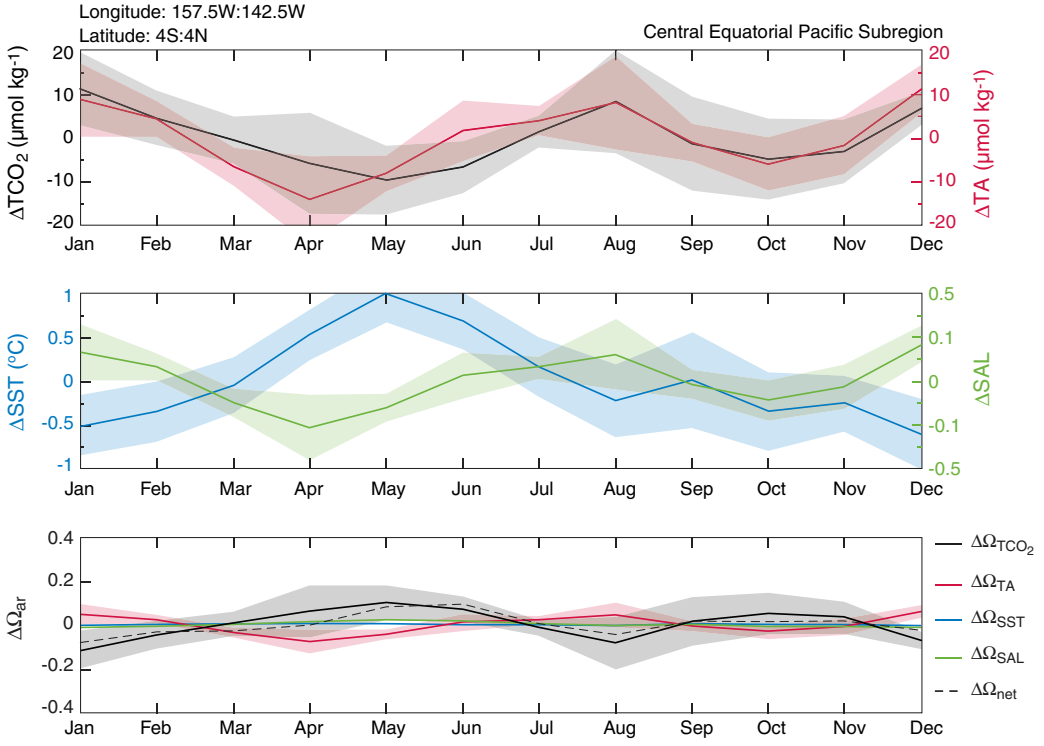

Fig. 10. In the Central Equatorial Pacific sub-region the seasonal variability with the annual mean removed in TCO_2 (black), TA (red), SST (blue), SAL (green), and their respective contribution to Ω_{ar}. The seasonality of the net effect of TCO_2, TA, SST, and SAL on Ω_{ar} is shown as a dashed line.

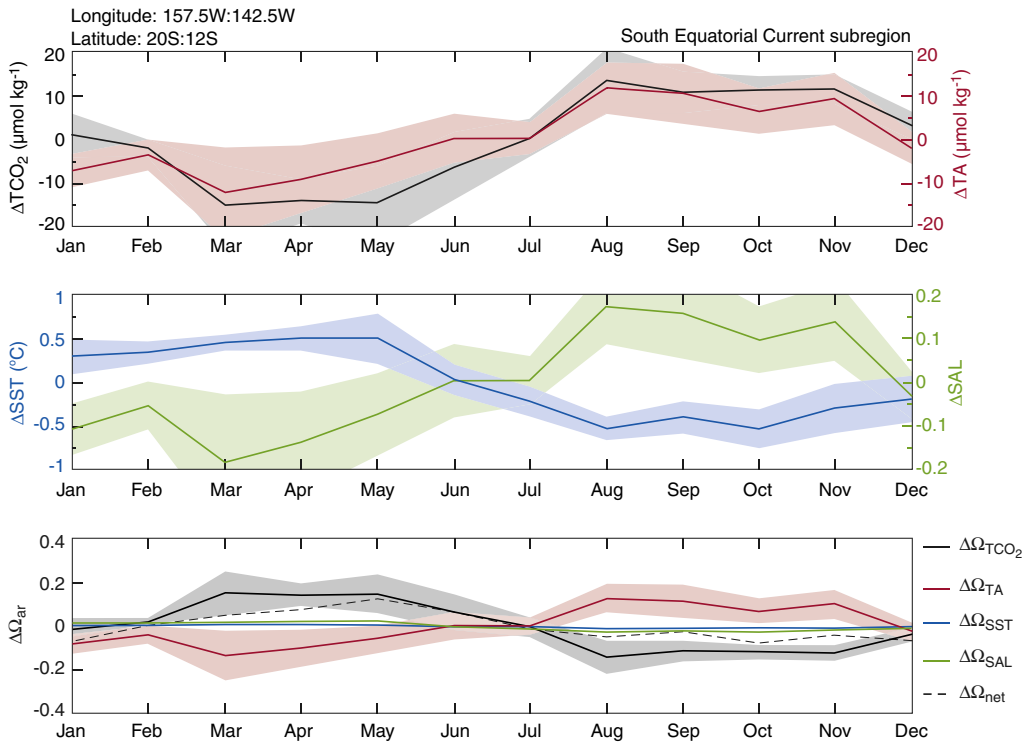

Fig. 11. In the South Equatorial Current sub-region the seasonal variability with the annual mean removed in TCO_2 (black), TA (red), SST (blue), SAL (green), and their respective contribution to Ω_{ar}. The seasonality of the net effect of TCO_2, TA, SST, and SAL on Ω_{ar} is shown as a dashed line.

and TA vary in the same way, TCO_2 decreases more than TA between March and July and increases more than TA between August and February. The decoupling of TCO_2 from TA results in an increase of Ω_{ar} between March and July, and a decrease between August and February.

The outgassing of CO_2 and vertical mixing are unlikely to cause the different changes in TCO_2 and TA for this region. The net sea–air flux of CO_2 in this region is close to zero (Takahashi et al., 2009). Vertical mixing or entrainment of waters has been shown to have a limited effect on the seasonal variability in salinity (Bingham et al., 2010). Vertical mixing or entrainment is also unlikely to have much of an impact on the seasonal variability in nitrate, which could drive some changes in TCO_2 relative to TA. These waters are oligotrophic (Behrenfeld et al., 2005) and seasonal changes in the biological drawdown of CO_2 are also expected to be low. Nitrate concentrations vary between 0.15 μmol kg^{-1} in the January to May period and 0.6 μmol kg^{-1} in the June–December (Garcia et al., 2010). Therefore the seasonal nitrate changes would only produce a decrease of 1 μmol kg^{-1} of TCO_2 in January–May and 4 μmol kg^{-1} in June–December, using the Redfield ratio. This would be less than 10% of the change calculated in TCO_2. Thus, we do not expect seasonal changes in biologically drawn down of CO_2, sea–air gas exchange, or vertical entrainment alone could explain the decoupling of the TCO_2 and TA signals.

Transport and evaporation seem to account for much of the variability in TCO_2 and TA in the SEC subregion (Fig. 11). The variabilities in TCO_2 and TA are coupled, and peak when the southeast trade winds are strongest in August, enhancing net evaporation (Bingham et al., 2010) and the westward flow of the SEC (Reverdin et al., 1994), both of which would increase SAL, TCO_2 and TA. The change in salinity through evaporation affects both TCO_2 and TA the same way and NTA is constant over time and space. The TCO_2/TA ratio in surface waters is greater in the eastern Pacific and greater transport of waters from the east from August to February could cause a net decrease in Ω_{ar}. This suggests that seasonal changes in the zonal transport of the SEC waters could account for a significant component of the seasonal change in Ω_{ar}.

4. Conclusion

The goal of this study was to investigate the variability in the aragonite saturation state (Ω_{ar}) at seasonal and basin scales for the Western Pacific (120°E:140°W and 35°S:30°N). We developed a new relationship between measured values of total alkalinity and salinity (Eq. (2)) to provide one of the key CO_2 system parameters needed to reconstruct and quantify the seasonal cycle of the aragonite saturation state. The TA–SAL relationship was found to be valid under all ENSO conditions and applicable across the entire study region. This relationship is an improvement of previous studies and provides a way to estimate high-resolution surface TA fields with salinity data from observational programs like ARGO (Gould et al., 2004). This updated relationship and the seasonal climatology of surface pCO_2 were used to calculate TCO_2 and Ω_{ar}.

The seasonal variability in Ω_{ar} is small in the Western Pacific Warm Pool and the North Equatorial Counter Current subregions because TA changes tend to offset the effect of TCO_2. Net precipitation changes in these two subregions drive the seasonal variabilities in TA and TCO_2. Vertical mixing is inhibited by the quasi-permanence of a barrier layer and the sea–air exchange of CO_2 and biological production were found to have only a small influence on the Ω_{ar} variability in the WPWP and NECC subregions. The variability in Ω_{ar} is larger in the Central Equatorial Pacific where the seasonal upwelling of waters with a higher TCO2/TA ratio than the surface waters causes decreases in Ω_{ar}. In the South Equatorial Current subregion, the seasonal variability in Ω_{ar} is also driven by greater changes in TCO_2 relative to TA. Seasonal shifts in net biological production and vertical mixing did not appear to drive the Ω_{ar} seasonality for the SEC. Net evaporation changes did alter TCO_2 and TA, but the changes in both parameters were similar with little influence on Ω_{ar}. Here, changes in the transport of waters higher in TCO_2 relative to TA

from the Eastern Pacific may provide a means to drive the seasonal variability in Ω_{ar}.

This study shows the seasonal variability in aragonite saturation state is small through most of the Pacific study region. The results do imply that many reefs in the region do not strongly influence the seasonality in Ω_{ar} of the open ocean, but large variability at reef scales does occur (Yates and Halley, 2006; Hofmann et al., 2011; Shaw et al., 2012; Kelly and Hofmann, 2013). Therefore, coastal and island scale studies are necessary to understand and quantify the impact of ocean acidification on the reef ecosystems of the region.

Acknowledgment

The research discussed in this paper was conducted with funding from the Pacific Climate Change Science Program to B. T. and the Pacific Climate Change Science and Adaptation Program to A. L. These programs were supported by AusAID, in collaboration with the Department of Climate Change and Energy Efficiency, and delivered by the Bureau of Meteorology and the Commonwealth Scientific and Industrial Research Organisation. We are grateful to Richard Matear and Bénédicte Pasquer for providing comments on earlier drafts.

References

Behrenfeld, M.J., Boss, E., Siegel, D.A., Shea, D.M., 2005. Carbon-based ocean productivity and phytoplankton physiology from space. Glob. Biogeochem. Cycles 19 (1). http://dx.doi.org/10.1029/2004GB00299.

Bingham, F.M., Foltz, G.R., McPhaden, M.J., 2010. Seasonal cycles of surface layer salinity in the Pacific Ocean. Ocean Sci. 6, 775–787. http://dx.doi.org/10.5194/os-6-775-2010.

Brewer, P.G., Goldman, J.C., 1976. Alkalinity changes generated by phytoplankton growth. Limnol. Oceanogr. 108–117.

Brown, J.R., et al., 2010. Evaluation of the South Pacific convergence zone in IPCC AR4 climate model simulations of the twentieth century. J. Clim. 24 (6), 1565–1582. http://dx.doi.org/10.1175/2010jcli3942.1.

Caldeira, K., Wickett, M.E., 2003. Oceanography: anthropogenic carbon and ocean pH. Nature 425 (6956), 365-365.

Cao, L., Caldeira, K., 2008. Atmospheric CO_2 stabilization and ocean acidification. Geophys. Res. Lett. 35 (19), L19609. http://dx.doi.org/10.1029/2008GL035072.

Chen, C.T.A., 1978. Decomposition of calcium carbonate and organic carbon in the deep oceans. Science 201 (4357), 735–736. http://dx.doi.org/10.1126/science.201.4357.735.

Chen, C.T., Millero, F.J., 1979. Gradual increase of oceanic carbon dioxide. Nature 277, 205–206.

Chen, C.T.A., Pytkowicz, R.M., 1979. On the total CO_2–titration alkalinity–oxygen system in the Pacific Ocean. Nature 281 (5730), 362–365. http://dx.doi.org/10.1038/281362a0.

Chen, S., Qiu, B., 2004. Seasonal variability of the South Equatorial Countercurrent. J. Geophys. Res. 109 (C8), C08003. http://dx.doi.org/10.1029/2003JC002243.

Christian, J.R., Feely, R.A., Ishii, M., Murtugudde, R., Wang, X., 2008. Testing an ocean carbon model with observed sea surface pCO_2 and dissolved inorganic carbon in the tropical Pacific Ocean. J. Geophys. Res. Oceans 113 (C7), C07047. http://dx.doi.org/10.1029/2007jc004428.

Cooley, S.R., Kite-Powell, H.L., Doney, S.C., 2009. Ocean acidification's potential to alter global marine ecosystem services. Oceanography 22 (4), 172–181.

Culkin, F., Cox, R.A., 1976. Sodium, potassium, magnesium, calcium and strontium in sea water. Deep Sea Res. Oceanogr. Abstr. 13 (5), 789–804. http://dx.doi.org/10.1016/0011-7471(76)90905-0.

De Boyer Montégut, C., Madec, G., Fischer, A.S., Lazar, A., Iudicone, D., 2004. Mixed layer depth over the global ocean: an examination of profile data and a profile-based climatology. J. Geophys. Res. 109, C12003. http://dx.doi.org/10.1029/2004JC002378.

De Boyer Montégut, C., Mignot, J., Lazar, A., Cravatte, S., 2007. Control of salinity on the mixed layer depth in the world ocean: 1. General description. J. Geophys. Res. 112 (C6), C06011. http://dx.doi.org/10.1029/2006JC003953.

Doney, S.C., et al., 2012. Climate change impacts on marine ecosystems. Ann. Rev. Mar. Sci. 4 (1), 11–37. http://dx.doi.org/10.1146/annurev-marine-041911-111611.

Dore, J.E., Lukas, R., Sadler, D.W., Church, M.J., Karl, D.M., 2009. Physical and biogeochemical modulation of ocean acidification in the central North Pacific. Proc. Natl. Acad. Sci. 106 (30), 12235–12240. http://dx.doi.org/10.1073/pnas.0906044106.

Dunn, J.R., Ridgway, K.R., 2002. Mapping ocean properties in regions of complex topography. Deep Sea Res. I 49 (3), 591–604. http://dx.doi.org/10.1016/s0967-0637(01)00069-3.

Fabry, V.J., Seibel, B.A., Feely, R.A., Orr, J.C., 2008. Impacts of ocean acidification on marine fauna and ecosystem processes. ICES J. Mar. Sci. 65 (3), 414–432. http://dx.doi.org/10.1093/icesjms/fsn048.

Feely, R.A., et al., 2002. Seasonal and interannual variability of CO_2 in the Equatorial Pacific. Deep Sea Res. II 49 (13–14), 2443–2469. http://dx.doi.org/10.1016/s0967-0645(02)00044-9.

Feely, R.A., Doney, S.C., Cooley, S.R., 2009. Ocean acidification: present conditions and future changes in a high-CO_2 world. Oceanography 22 (4), 36–47.

Feely, R.A., et al., 2012. Decadal changes in the aragonite and calcite saturation state of the Pacific Ocean. Glob. Biogeochem. Cycles 26 (3), GB3001. http://dx.doi.org/10.1029/2011gb004157.

Ganachaud, A., et al., 2012. Vulnerability of Fisheries and Aquaculture in the Tropical Pacific to Climate Change. In: Bell, J.D., Johnson, J.E., Hobday, A.J. (Eds.), Secretariat of the Pacific Community.

Garcia, H.E., et al., 2010. World Ocean Atlas 2009. Volume 4: Nutrients (Phosphate, Nitrate, Silicate)NOAA Atlas NESDIS 71, U.S. Government Printing Office, Washington, D.C.

Gattuso, J.P., Frankignoulle, M., Bourge, I., Romaine, S., Buddemeier, R.W., 1998. Effect of calcium carbonate saturation of seawater on coral calcification. Glob. Planet Change 18 (1–2), 37–46. http://dx.doi.org/10.1016/s0921-8181(98)00035-6.

Gould, J., et al., 2004. Argo profiling floats bring new era of in situ ocean observations. Eos Trans. AGU 85 (19). http://dx.doi.org/10.1029/2004eo190002.

Guinotte, J., Buddemeier, R., Kleypas, J., 2003. Future coral reef habitat marginality: temporal and spatial effects of climate change in the Pacific basin. Coral Reefs 22, 551–558. http://dx.doi.org/10.1007/s00338-003-0331-4.

Hoegh-Guldberg, O., et al., 2007. Coral reefs under rapid climate change and ocean acidification. Science 318 (5857), 1737. http://dx.doi.org/10.1126/science.1152509.

Hofmann, G.E., et al., 2011. High-frequency dynamics of ocean pH: a multi-ecosystem comparison. PLoS ONE 6 (12), e28983. http://dx.doi.org/10.1371/journal.pone.0028983.

Iglesias-Rodriguez, M.D., et al., 2008. Phytoplankton calcification in a high-CO_2 world. Science 320 (5874), 336–340. http://dx.doi.org/10.1126/science.1154122.

Inoue, H.Y., et al., 1995. Long-term trend of the partial pressure of carbon dioxide (pCO_2) in surface waters of the western North Pacific, 1984–1993. Tellus B 47 (4), 391–413. http://dx.doi.org/10.1034/j.1600-0889.47.issue4.2.x.

Inoue, H.Y., et al., 2003. Distribution of the partial pressure of CO_2 in surface water (pCO_2^w) between Japan and the Hawaiian Islands: pCO_2^w–SST relationship in the winter and summer. Tellus B 55 (2), 456–465. http://dx.doi.org/10.1034/j.1600-0889.2003.01482.x.

Ishii, M., et al., 2001. Seasonal variation in total inorganic carbon and its controlling processes in surface waters of the western north pacific subtropical gyre. Mar. Chem. 75 (1–2), 17–32. http://dx.doi.org/10.1016/S0304-4203(01)00023-8.

Ishii, M., et al., 2009. Spatial variability and decadal trend of the oceanic CO_2 in the Western Equatorial Pacific warm/fresh water. Deep Sea Res. II 56 (8–10), 591–606. http://dx.doi.org/10.1016/j.dsr2.2009.01.002.

Johnson, G.C., Sloyan, B.M., Kessler, W.S., McTaggart, K.E., 2002. Direct measurements of upper ocean currents and water properties across the tropical Pacific during the 1990s. Prog. Oceanogr. 52 (1), 31–61. http://dx.doi.org/10.1016/s0079-6611(02)00021-6.

Kelly, M.W., Hofmann, G.E., 2013. Adaptation and the physiology of ocean acidification. Funct. Ecol. 27 (4), 980–990. http://dx.doi.org/10.1111/j.1365-2435.2012.02061.x.

Key, R., et al., 2004. A global ocean carbon climatology: results from Global Data Analysis Project (GLODAP). Glob. Biogeochem. Cycles 18 (4). http://dx.doi.org/10.1029/2004GB002247.

Kleypas, J.A., McManus, J.W., Menez, L.A.B., 1999. Environmental limits to coral reef development: where do we draw the line? Am. Zool. 39 (1), 146–159. http://dx.doi.org/10.1093/icb/39.1.146.

Kobashi, F., Kawamura, H., 2002. Seasonal variation and instability nature of the North Pacific Subtropical Countercurrent and the Hawaiian Lee Countercurrent. J. Geophys. Res. 107 (C11), 3185. http://dx.doi.org/10.1029/2001JC001225.

Langdon, C., Atkinson, M.J., 2005. Effect of elevated pCO_2 on photosynthesis and calcification of corals and interactions with seasonal change in temperature/irradiance and nutrient enrichment. J. Geophys. Res. 110 (C9), C09S07. http://dx.doi.org/10.1029/1999GB001195.

Langdon, C., et al., 2000. Effect of calcium carbonate saturation state on the calcification rate of an experimental coral reef. Glob. Biogeochem. Cycles 14 (2), 639–654. http://dx.doi.org/10.1029/1999GB001195.

Le Borgne, R., Feely, R.A., Mackey, D.J., 2002. Carbon fluxes in the equatorial pacific: a synthesis of the JGOFS programme. Deep Sea Res. II 49 (13–14), 2425–2442. http://dx.doi.org/10.1016/s0967-0645(02)00043-7.

Lee, K., et al., 2006. Global relationships of total alkalinity with salinity and temperature in surface waters of the world's oceans. Geophys. Res. Lett. 33 (19), L19605. http://dx.doi.org/10.1029/2006GL027207.

McPhaden, M.J., 1999. Genesis and evolution of the 1997–98 El Niño. Science 283 (5404), 950–954. http://dx.doi.org/10.1126/science.283.5404.950.

McPhaden, M., Picaut, J., 1990. El Niño-southern oscillation displacements of the Western equatorial Pacific warm pool. Science 250 (4986), 1385–1388. http://dx.doi.org/10.1126/science.250.4986.1385.

Millero, F.J., Lee, K., Roche, M., 1998. Distribution of alkalinity in the surface waters of the major oceans. Mar. Chem. 60 (1–2), 111–130. http://dx.doi.org/10.1016/S0304-4203(97)00084-4.

Millero, F.J., Graham, T.B., Huang, F., Bustos-Serrano, H., Pierrot, D., 2006. Dissociation constants of carbonic acid in seawater as a function of salinity and temperature. Mar. Chem. 100 (1–2), 80–94. http://dx.doi.org/10.1016/J.Marchem.2005.12.001.

Mucci, A., 1983. The solubility of calcite and aragonite in seawater at various salinities, temperatures, and one atmosphere total pressure. Am. J. Sci. 283 (7), 780–799.

Nakicenovic, N., et al., 2000. Special report on emissions scenarios. Special Report of Working Group III of the Intergovernmental Panel on Climate Change. Cambridge University Press.

Orr, J.C., et al., 2005. Anthropogenic ocean acidification over the twenty-first century and its impact on calcifying organisms. Nature 437 (7059), 681–686. http://dx.doi.org/10.1038/nature04095.

Park, P.K., 1969. Oceanic CO_2 system: an evaluation of ten methods of investigation. Limnol. Oceanogr. 14 (2), 179–186.

Philander, S.G.H. (Ed.), 1990. El Niño, La Niña and the Southern Oscillation. Academic Press, Inc., San Diego, California. [92101, 289 pp.].

Philander, S.G.H., Hurlin, W.J., Seigel, A.D., 1987. Simulation of the seasonal cycle of the tropical Pacific Ocean. J. Phys. Oceanogr. 17 (11), 1986–2002. http://dx.doi.org/10.1175/1520-0485(1987) 017<1986:sotsco>2.0.co;2.

Reverdin, G., Frankignoul, C., Kestenare, E., McPhaden, M.J., 1994. Seasonal variability in the surface currents of the equatorial Pacific. J. Geophys. Res. 99 (C10), 20323–20344. http://dx.doi.org/10.1029/94JC01477.

Ridgway, K.R., Dunn, J.R., Wilkin, J.L., 2002. Ocean interpolation by four-dimensional weighted least squares—application to the waters around Australasia. J. Atmos. Ocean. Technol. 19 (9), 1357–1375. http://dx.doi.org/10.1175/1520-0426(2002)019<1357:oibfdw>2.0.co;2.

Sabine, C.L., Feely, R.A., Gruber, N., Key, R.M., Lee, K., Bullister, J.L., Wanninkhof, R., Wong, C.S., Wallace, D.W.R., Tilbrook, B., Millero, F.J., Peng, T.-H., Kozyr, A., Ono, T., Rios, A.F., 2004. The oceanic sink for anthropogenic CO2. Science 305 (5682), 367–371. http://dx.doi.org/10.1126/science.1097403.

Shaw, E., McNeil, B., Tilbrook, B., 2012. Impacts of ocean acidification in naturally variable coral reef flat ecosystems. J. Geophys. Res. Oceans 117 (C03038), 14pp. http://dx.doi.org/10.1029/2011jc007655.

Silverman, J., Lazar, B., Cao, L., Caldeira, K., Erez, J., 2009. Coral reefs may start dissolving when atmospheric CO_2 doubles. Geophys. Res. Lett. 36 (5), L05606. http://dx.doi.org/10.1029/2008GL036282.

Stanley, S.M., Hardie, L.A., 1998. Secular oscillations in the carbonate mineralogy of reef-building and sediment-producing organisms driven by tectonically forced shifts in seawater chemistry. Palaeogeogr. Palaeoclimatol. Palaeoecol. 144 (1–2). http://dx.doi.org/10.1016/s0031-0182(98)00109.

Takahashi, T., et al., 2009. Climatological mean and decadal change in surface ocean pCO_2, and net sea–air CO_2 flux over the global oceans. Deep Sea Res. II 56 (8–10), 554–577. http://dx.doi.org/10.1016/j.dsr2.2008.12.009.

Takahashi, T., Sutherland, S.C. and Kozyr, A., 2010. Global ocean surface water partial pressure of CO_2 database: measurements performed during 1957–2009 (Version 2009). In: O.R.N.L. Carbon Dioxide Information Analysis Center, U.S. Department of Energy (Editor).

Van Heuven, S., Pierrot, D., Lewis, E., Wallace, D.W.R., 2009. MATLAB Program Developed for CO_2 System Calculations, ORNL/CDIAC-105b. Carbon Dioxide Information Analysis Center Oak Ridge National Laboratory. U.S. Department of Energy, Oak Ridge, Tennessee.

Wang, B., Wu, R., Lukas, R., 2000. Annual adjustment of the thermocline in the tropical Pacific Ocean. J. Clim. 13 (3), 596–616. http://dx.doi.org/10.1175/1520-0442(2000) 013<0596:aaotti>2.0.co;2.

Wanninkhof, R., et al., 1995. Seasonal and lateral variations in carbon chemistry of surface water in the Eastern Equatorial Pacific during 1992. Deep Sea Res. II 42 (2–3), 387–409. http://dx.doi.org/10.1016/0967-0645(95)00016-j.

Yates, K.K., Halley, R.B., 2006. CO_3^{2-} concentration and pCO_2 thresholds for calcification and dissolution on the Molokai reef flat, Hawaii. Biogeosciences 3 (3), 357–369. http://dx.doi.org/10.5194/bg-3-357-2006.